

Modeling Volume Changes and High Temperature Microstructure in Cast Iron

A. Starobin, M. C. Carter

March 2011

The cast iron model in *FLOW-3D*¹ version 10.0 tracks density changes in the liquid iron and during iron freezing and predicts the high temperature microstructure comprised of graphite, austenite and carbide phases. The model uses a realistic iron freezing path and a chilling susceptibility criterion that controls the local amount of carbide formation.

One of the main concerns of a foundry engineer is excessive shrinkage porosity that may form during solidification. Most of the volumetric changes in cast irons take place during cooling of the liquid alloy from the pouring temperature to the solidus and, more significantly, during eutectic solidification, when gamma-iron, graphite and carbide form. The placing of risers (or *risering*) provides additional metal to feed the shrinkage. Optimum risering is important for achieving good quality casting at the minimum cost. The amount of shrinkage can also be controlled by proper alloying and cooling of the metal. The cast iron model in *FLOW-3D* takes into account all these factors to predict the formation of porosity and the development of the phases during eutectic solidification.

Model Overview

Cast iron is a near-eutectic iron alloyed with carbon and silicon. Carbon is typically present in the range from 2.5 wt % to 4.5 wt % and silicon in the range from 1 wt % to 3 wt %. Silicon is added to stabilize graphite and to reduce “chilling” tendency (i.e., the formation of carbidic iron). Other elements and compounds are present in trace amounts and typically either control the graphite shape (e.g., magnesium in ductile iron), act as additional deoxidizers, (e.g., phosphorous), or serve as inoculants of graphite (e.g., ferro-silicon).

The *FLOW-3D* cast iron model accounts for the volume changes occurring from the pouring temperature to the solidus: the shrinkage of the metal during cooling in the liquid state; further shrinkage during pre-eutectic gamma iron formation; subsequent shrinkage or expansion during the eutectic reaction; and the secondary shrinkage from the end of the eutectic reaction to the solidus. Since cast iron typically contains non-iron phases that include silicon oxide, phosphorous oxide, manganese sulfide and nitrogen and hydrogen microporosity, a heuristic allowance is made for the effect of these phases on the density of the solidified metal.

¹ *FLOW-3D* is a registered trademark in the USA and other countries.

The latent heat release in the cast iron solidification model is computed as a function of temperature (the so-called freezing path) determined from the Fe-C phase diagram [13], using the initial concentration of carbon and silicon in the melt. The model can be used together with the general solidification model in *FLOW-3D*, with or without flow. However, volume changes associated with the formation of different phases *are only coupled to the simplified shrinkage model which does not include flow*.

The effect of mold wall movement during iron expansion is not included in the present model. Any net volume expansion that cannot be accommodated by the available space in the mold is ignored.

Microstructure is computed only insofar as it controls density changes during liquid cooling and metal freezing. In the eutectic region the speed of the eutectic front is used to compute the local chilling tendency, and, therefore, the local amount of carbide formation. Thus modeling of chill zones near mold walls is possible. No attempt is made to track further decomposition of the gamma phase or the carbides during the solid-state eutectoid transformation. Therefore, a complete picture of the final cast microstructure is not predicted.

For hyper-eutectic cast irons it is assumed that only graphite forms during the initial pre-eutectic stage of solidification, as in gray and ductile irons. In other words, the model does not include the solidification of hyper-eutectic white irons during the initial pre-eutectic stage in which primarily carbide forms.

Theory Behind the Model: Iron Freezing Path

The cast iron freezing path is that of a eutectic alloy. It can be characterized by the liquidus temperature, eutectic temperature, the eutectic-start and eutectic-end solid fractions and the solidus temperature. All, but the last two quantities are computed from the equilibrium ternary Fe-C-Si phase diagram [13].

The primary high temperature solid phases formed during freezing are the gamma iron, or austenite (a carbon-iron solution) and graphite. The carbon solubility in the gamma phase depends on the Si content and is written as:

$$C_{\gamma, mx} = 2.07 - 0.098 Si \quad (1)$$

in close agreement with the solubility line reported by Stefanescu [7]. The liquidus of the alloy follows from either the hypo-eutectic liquidus plane:

$$T_l = 1636 - 113 (C + 0.25 Si) \quad (2)$$

or the hyper-eutectic liquidus plane [7]:

$$T_l = -505.8 + 389.1(C + 0.31 Si) \quad (3)$$

and the eutectic compositions and temperatures are given by the intersection of these planes:

$$C_e = 4.26 - 0.296 Si \quad (4)$$

$$T_e = 1154.6 + 5.2 Si. \quad (5)$$

The beginning of the eutectic reaction is a derived quantity given by the lever rule:

$$f_e = \frac{C - C_e}{C_{\gamma, mx} - C_e} \quad (6)$$

The measurements in [6] suggest this form is accurate for a number of cast irons.

Since no attempt is made to account for the cast iron thermodynamics beyond the influence of the primary alloying elements, both the end of graphitic eutectic reaction, f_{ee} , and the solidus, T_s , are left as user-defined quantities. The simplest cast iron freezing path would have $T_s = T_e$ and $f_{ee} = 1$. If one considers positive segregation of phosphorous in the liquid, the actual solidus temperature is below the graphitic eutectic temperature, and can be as low as 1100 °C. For this case, it is assumed that graphite precipitation is complete before the end of freezing, and that the last fraction of metal to freeze, $1 - f_{ee}$, does so at a density ρ_{ei} , different from the eutectic density.

Figure 1 shows a computed iron freezing path. The example iron has 3.4 wt % carbon and 2.5 wt % silicon. The carbon equivalent ($CE = C + 0.296 Si$) for this hypo-eutectic iron is 4.0 %, the liquidus from equation (2) is 1180 °C. The eutectic temperature and carbon concentration from equations (5) and (6) are 1168 °C and 3.52 wt %. The maximum carbon solubility in the gamma phase is 1.83 wt % from equation (1), and finally from equation (6) the eutectic-start solid fraction is 6.6 wt % . The eutectic-end solid fraction is set to 99% and the solidus is set equal to 1100 °C.

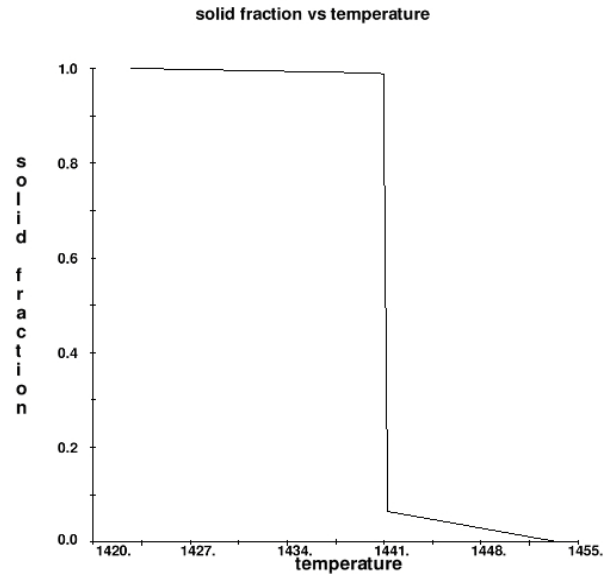


Figure 1: Model freezing path for a sample iron with 3.4 wt % carbon and 2.5 wt % silicon. Temperature in degrees K.

Equilibrium Iron Density Changes

For sufficiently slow eutectic freezing rates no carbide forms and the equilibrium phases prevail. In cast iron, the superheats are large, the liquid shrinkage is sizeable, and, depending on the pour temperature, the net volume change could be either positive or negative. The temperature dependence of the density of liquid iron is modeled in a linear form as:

$$\rho(T) = \rho_0(1 - \alpha(T - T_0)). \quad (7)$$

or by defining the function $\rho(T)$ in a tabular form. The values for the reference density, ρ_0 , reference temperature, T_0 and the expansion coefficient, α , derived from the German Foundry Society data (VDG) [1,2,8] are 6.75 g/cc, 1400 °C and $2.3 \times 10^{-4} \text{ } ^\circ\text{C}^{-1}$, respectively. Thus, for the example iron alloy in the previous section with a 220 °C superheat, the liquid will shrink by 4.8% even before reaching the liquidus.

Once in the freezing range, gamma iron forms until f_e solid fraction is reached. The density value of this phase, ρ_γ , consistent with the available data is 7.2 g/cc [1,2,9]. Subsequently, the regular eutectic solid is at the mean carbon concentration of C_e and gamma/graphite partition in this phase follows the lever rule:

$$\begin{aligned} \phi_\gamma C_{\gamma, mx} + \phi_g 100 &= C_e, \\ \phi_\gamma + \phi_g &= 1, \end{aligned} \quad (8)$$

where ϕ_γ and ϕ_g are gamma and graphite eutectic weight fractions. This gives for ϕ_γ and the density of the eutectic phase ρ_{es} :

$$\phi_\gamma = \frac{C_e - 100}{C_{\gamma, mx} - 100}, \quad \rho_{es}^{-1} = \frac{\phi_\gamma}{\rho_\gamma} + \frac{\phi_g}{\rho_g} \quad (9)$$

Graphite density is taken at 2.2 g/cc and the value of the eutectic for the considered composition is 6.9 g/cc. In contrast, the coherent crystallographic graphite density taken at the eutectic temperature is 2.6 g/cc [11]. However, cast iron graphite is far from a perfect crystal and should have a lower density due to grain boundaries and other imperfections in its structure.

For the overall volume change we can write:

$$\Delta v = \frac{\rho_1(T)}{\rho_s} - 1, \quad \rho_s^{-1} = \frac{f_e}{\rho_\gamma} + \frac{f_{ee} - f_e}{\rho_{se}} + \frac{1 - f_{ee}}{\rho_{ei}}. \quad (10)$$

For the simplest freezing path with $f_{ee} = 1$, the last term in equation (10) is zero. In this case only gamma and graphite phases are allowed to form in the iron. The two-phase

limit of the model is compared in Table 1A against AFS/VDG volume change data [1] for irons of different compositions (columns 3 and 5). The model systematically over-predicts the amount of shrinkage. An adjustment of gamma and graphite densities from the values of 7.2 g/cc and 2.2 g/cc did not lead to significant improvement in the agreement with data.

When additional phases with the mean density of 4.1 g/cc were added to the model and the eutectic-end solid fraction was allowed to increase with the carbon content as $f_{ee} = \min(1, 0.956 + 10^{-2}C)$ (C is wt % of carbon), a near perfect agreement with the AFS/VDG data was seen. That the higher carbon irons appear to freeze with fewer non-primary phases is plausible due to the significant reduction of liquid iron nitrogen and hydrogen solubility associated with the addition of carbon [11]. The density of 4.1 g/cc is in the range of the densities of forming non-primary phases (in g/cc: $SiO_2 \sim 2.4$, $Fe_3P \sim 6.3$, $MnS \sim 3.6$) and is also plausible. Precipitation of some of the oxides is also known to occur above the liquidus of iron. Thus the inclusion of these in the end-of-freezing solid fraction range between f_{ee} and 1 is a further simplification.

In Table 1B the sample iron is modeled with different pour temperatures. Higher pour temperatures lead to higher overall shrinkage, and the agreement between the model and the data is found satisfactory over a 300 °C pour temperature range.

Figure 2 shows iron volume history curves for iron poured at three temperatures: 1250, 1400 and 1550 °C. At the lowest pour temperature the iron expands overall, while for a 1400 and 1550 °C pour there is net shrinkage. The inflection points correspond to the beginning of the eutectic reaction with graphite precipitation.

Table 1A. Measured and computed equilibrium volume change for iron plates with different compositions. Iron plate modulus is 60 mm and the iron is poured at 1400 °C.

C	Si	Shrinkage - % with $f_{ee} = 1$	Shrinkage - % with $f_{ee} = 0.956 + 10^{-2}C$	AFS/VDG [1] shrinkage - %
4	1.5	-1.26	-0.96	-0.93
3.4	2.5	-2.4	-1.66	-1.74
2.8	3.5	-3.2	-2.4	-2.4
2.8	1.5	-4	-2.8	-2.7

Table 1B. Equilibrium volume change for three pouring temperatures for an iron with carbon content of 3.4 wt % and silicon content of 2.5 wt %

Pour Temperature (°C)	Shrinkage - %	AFS/VDG shrinkage - %
1250	+1.66	+1.38
1400	-1.66	-1.7
1550	-4.8	-4.8

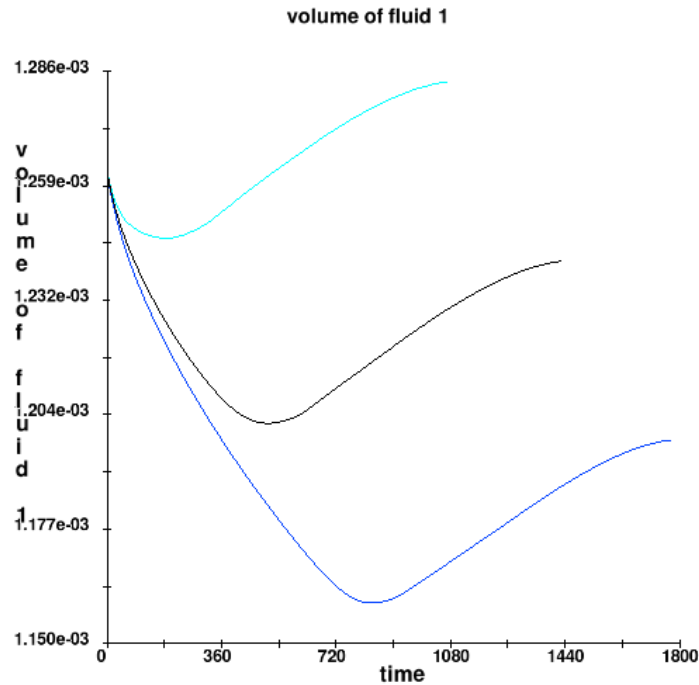


Figure 2. Computed volume vs. time for three pouring temperatures (iron in Table 1B). From shortest to longest freeze time (top to bottom): 1250, 1400 and 1550 °C pour.

Non-Equilibrium Iron Density Changes and the Chilling Susceptibility Model

In thinner casting sections some white iron (or “chill”) will form. The microscopic mechanism for chill formation is described by Kurz [4]. A regular (white) eutectic and an irregular grey eutectic grow competitively. At high freezing rates the white eutectic is stable in part due to shallower carbon concentration gradients ahead of the eutectic front. At lower cooling rates grey eutectic is stable.

The transition is hysteretic for it is harder to nucleate a grey eutectic cell ahead of the regular white eutectic and the white-to-grey transition speed is measured to be $\sim 10 \frac{\mu m}{s}$. The reverse transition is observed at approximately $100 \frac{\mu m}{s}$ [3,4]. The actual values will depend on inoculation and specific composition of cast iron.

To account for chill formation in the model we adopt a somewhat simpler view of the physics. In a range of freezing front speeds, $v_e \in \left[\frac{v_-}{\chi_{eut}}, \frac{v_+}{\chi_{eut}} \right]$ amount of chill formed varies from zero to maximum allowed, $\phi_{c, mx}$, for a given composition. $v_- = 30 \frac{\mu m}{s}$, $v_+ = 60 \frac{\mu m}{s}$ and χ_{eut} is the chilling susceptibility coefficient, a user-defined parameter with values in the range from 0.0 to 1.0 with the default value of 1.0. For well-inoculated iron, or for a grey eutectic with a high specific surface area, χ_{eut} is close to zero and no chill will form. On the other hand, if the iron is un-inoculated the default value of one should be more appropriate. The actual value of χ_{eut} must be determined from the results of a specific ASTM chill-wedge test (see below).

The maximum amount of carbide will form if no graphite precipitates in the eutectic region. Then the two eutectic phases, gamma and stoichiometric carbide, Fe_3C , form in proportion given by the lever rule:

$$\begin{aligned} \phi_\gamma C_{\gamma, mx} + \phi_{c, mx} 6.69 &= C_e, \\ \phi_\gamma + \phi_{c, mx} &= 1, \end{aligned} \quad (11)$$

where 6.69 is the stoichiometric carbon content in carbide, and $\phi_{c, mx}$ is given by:

$$\phi_{c, mx} = \frac{C_{\gamma, mx} - C_e}{C_{\gamma, mx} - 6.69}. \quad (12)$$

The chill formation law is then:

$$\begin{aligned} \phi_c &= 0, \quad v_e < \frac{v_-}{\chi_{eut}} \\ \phi_c(v_e) &= \phi_{c, mx} \left(\frac{\chi_{eut} v_e - v_-}{v_+ - v_-} \right)^{0.25}, \quad v_e \in \left[\frac{v_-}{\chi_{eut}}, \frac{v_+}{\chi_{eut}} \right] \\ \phi_c &= \phi_{c, mx}, \quad v_e > \frac{v_+}{\chi_{eut}}. \end{aligned} \quad (13)$$

The exponent of 0.25 is in agreement with the model of Fraz that predicts the amount of chill in iron wedges [3].

The density of a three-phase eutectic follows from a modified lever rule:

$$\begin{aligned} \phi_\gamma C_{\gamma, mx} + \phi_g 100 &= C_e - \phi_c(v_s) 6.69, \\ \phi_\gamma + \phi_g &= 1 - \phi_c(v_s) \end{aligned} \quad (14)$$

and

$$\phi_{\gamma} = \frac{(C_e - \phi_c 6.69) - (1 - \phi_c) 100}{C_{\gamma, mx} - 100}, \quad \rho_{es}^{-1} = \frac{\phi_{\gamma}}{\rho_{\gamma}} + \frac{\phi_{\gamma}}{\rho_c} + \frac{\phi_{\gamma}}{\rho_g}. \quad (15)$$

At intermediate freezing rates the volume changes predicted by the model with the AFS/VDG data were compared again. Freezing of plates of different moduli is simulated at a number of resolutions and the results are summarized in Table 2. In Figure 3 the carbide and graphite fields at the end of freezing for an 8 mm modulus plate are plotted. The simulated iron has the same composition and freezing path as in the previous sections. The pour temperature is still 1400 °C, and the suitable value of χ_{eut} for VDG irons is 0.9.

Solidification becomes progressively more carbidic as the modulus is reduced from 40 mm to 1 mm. For the 40 mm modulus, freezing is essentially equilibrium, while for the 1 mm modulus most of the iron formed is white. In the carbidic limit, the AFS/VDG shrinkage is composition independent because the carbide and gamma densities are very similar (~ 7.2 g/cc). Further, in the carbidic, or quench limit, microporosity and non-primary phases do not form [10]. Thus, for fast freezing parts of the casting, the density of the phase forming between f_{ee} and 1 should be close to the gamma density. For simplicity, the following linear relationship was adopted:

$$\rho_{ei,*} = \frac{\phi_c}{\phi_{c, mx}} (\rho_{\gamma} - \rho_{ei}) + \rho_{ei} \quad (16)$$

where $\rho_{ei,*}$ is the actual post-eutectic density used to model volume change.

The agreement between the model and the data is satisfactory. Because the chill model relies on the numerical estimate of the freezing front speed, some mesh sensitivity is observed in the results. This is especially true at the intermediate moduli.

Table 2. Carbide formation and shrinkage in plates of different moduli (1400 °C pour, 3.4 wt % C, 2.5 wt % Si, $\chi_{eut} = 0.9$, $\phi_{c, mx} = 32\%$)

Modulus (mm)	Resolution (mm)	Shrinkage % (computed)	AFS/VDG shrinkage [1]	Carbides wt % (computed)	Graphite wt % (computed)
40	6	-2.24	-1.7	3.80	1.4
40	2	-1.9	-1.7	1.60	1.5
8	4	-4.0	-3.8	17.0	0.75
8	3	-3.6	-3.8	14.2	0.88
8	2	-3.4	-3.8	12.8	0.94
8	1	-3.3	-3.8	11.6	1.0
1	0.3	-5.5	-5.4	31.5	0.035
1	0.15	-5.5	-5.4	30.5	0.083

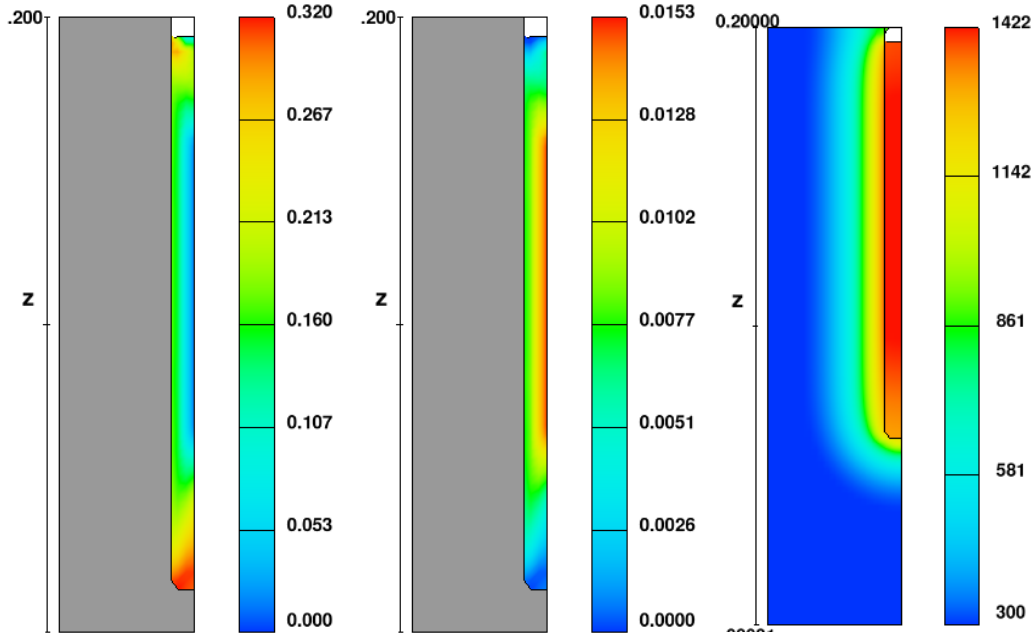


Figure 3. End-of-freezing carbide and graphite Wt% in an 8 mm modulus plate (left-most and center panel). Temperature in the plate and the mold at the end of freezing (right panel, with temperature in degrees K).

ASTM A367 Data Comparison

The ASTM A367 standard (25 mm at base x 44 mm section height x 144 mm length) is used to check for chill susceptibility of a given batch of foundry iron. It is also used to check efficacy of an inoculation agent. A detailed report on the behavior of a specific iron (3.4 wt % C, 1.7 wt % Si, 0.75 wt % Mn, 0.02 wt % S, 0.12 wt % P) is available from Chisamer, et al. [5]. They measure the amount of chill in un-inoculated and ferrosilicon inoculated iron. Measurements are done for carbide weight fraction along the midline of the wedge. The model captures this data well. The comparison is shown in Table 3A-C. Figure 3 shows computed phase fields for un-inoculated iron and at 0.2 wt % of FeSi7.5 inoculation. For each level of inoculation, a distinct value of χ_e is found that allows a match with data.

Table 3A-C. Midsection carbide content for un-inoculated and inoculated irons, comparison with data in [5].

A. Un-inoculated ($\chi_{eut} = 0.40$)

Distance From Apex (mm)	Carbide Content (%)	Measured (%) [5]
5	30	35
25	17	15
40	7	5

B. 0.1 % FeSi7.5 ($\chi_{eut} = 0.37$)

Distance From Apex (mm)	Carbide Content (%)	Measured (%) [5]
5	30	30
25	10	10
40	4	5

C. 0.2% of FeSi7.5 ($\chi_{eut} = 0.25$).

Distance From Apex (mm)	Carbide Content (%)	Measured (%) [5]
5	27	30
25	4	5
40	0	5

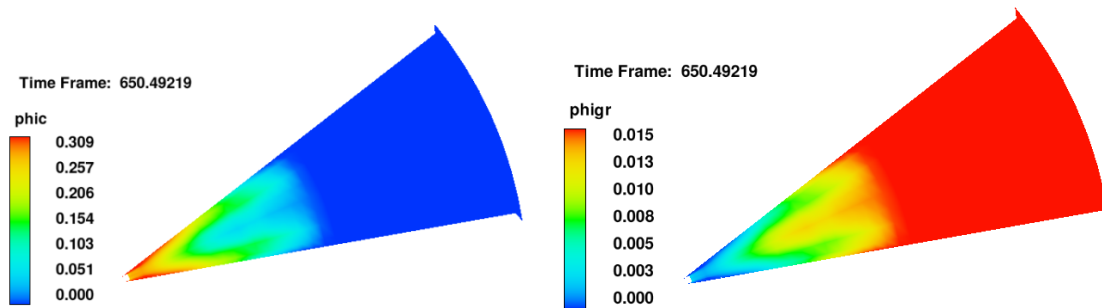


Figure 4A. Carbide and graphite content in an inoculated iron.

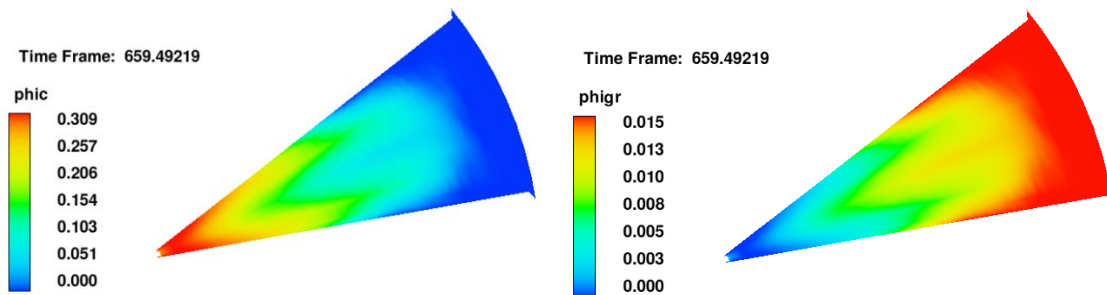


Figure 4B. Carbide and graphite content in an un-inoculated iron.

Summary

A cast iron model is described for tracking density changes in iron during freezing and for predicting the microstructure that contains graphite, austenite and carbide phases. This model is an option to the simple solidification shrinkage model which does not include fluid flow. It can also be used during solidification, with or without flow, to better define heats of transformation in iron with high (> 2%) carbon content. Both shrinkage and expansion are included in the simple shrinkage model, except when there is no space for expansion in which case the expansion is ignored.

Table 4 lists the input variables required in *FLOW-3D* to use the cast iron model.

Table 4. Summary of *FLOW-3D* input variables unique to the iron model.

Description	Tech Note Symbol	<i>FLOW-3D</i> Variable	Namelist
Global model flag		IFIRON	XPUT
Carbon content	C	CIRON	PROPS
Silicon content	Si	SIIRON	PROPS
Gamma iron density	ρ_γ	RHOGAMMA	PROPS
Graphite density	ρ_g	RHOGRPAHITE	PROPS
Solid density formed above FSEUTE	ρ_{ei}	RHOENDIRON	PROPS
Solid fraction at the end of graphitic eutectic reaction	f_{ee}	FSEUTE	PROPS
Carbide density	ρ_c	RHOCARBIDE	PROPS
Inoculation/chilling tendency parameter	χ_{eut}	VSEUTPHI	PROPS

References

- [1] AFS, *Gating Calculations for Iron Castings*, spreadsheet, 2009.
- [2] Von Alfred Holzmuller, VDG and Robert Wlodawer, VDG, "Zehn Jahre Speiser-Eingriffs-Verfahren fur Guseisen," Giesserei, 1963.
- [3] Fras and Lopez, "A Theoretical analysis of the chilling susceptibility of hypoeutectic Fe-C alloys," Acta. Metal. Mater., 1993.
- [4] Magnin and Kurz, "Competitive growth of stable and meta-stable Fe-C-X eutectics: Part II. Mechanisms," Met. Trans. A, 1987.
- [5] Chisamer, et al., "Comparison of Oxy-sulfide Alloy Tablets and Ca-bearing FeSi7.5 for late inoculation of low sulfur grey irons," AFS Transactions, 2007.

- [6] K.G. Upadhyaya, D.M. Stefanescu, K. Lieu and D.P. Yeager, "Computer-Aided Cooling Curve Analysis: Principles and Applications in Metal Casting", AFS Transactions, Vol. 97, 1989, 61-66.
- [7] D. M. Stefanescu, S. Katz, "Thermodynamic Properties of Iron-Base Alloys," ASM Handbook Volume 15, Casting (ASM International), 2008
- [8] K. Grutter and B. Mairincek. Arch. Eisenhüttenwes. 24 (9-10), 447, 1954.
- [9] G. Goodrich. *Introduction to cast irons*. ASM Handbook, 2008, Volume 15: Casting. pp. 794-795.
- [10] A. Buhrig-Polackzek and D. Santos, "Solidification of Eutectic Alloys – Cast Iron," ASM Handbook, Volume 15: Casting, pp.317-329.
- [11] R. Fruehan, "Gases in Metals," ASM Handbook, 2008, Volume 15: Casting, pp.82-87.
- [12] P. Wray, "Predicted Volume Change Behavior Accompanying the Solidification of Binary Alloys," Met. Trans. B, 7B, December, 1976.
- [13] G. Goodrich and John Svoboda, "Basic Concepts of Ferrous Metallurgy," Cast Metals Institute, Inc. 1997, American Foundry Society, Inc.